AIAA JOURNAL
Vol. 40, No. 10, October 2002

Technical Notes

TECHNICAL NOTES are short manuscripts describing new developments or important results of a preliminary nature. These Notes cannot exceed six manuscript pages and three figures; a page of text may be substituted for a figure and vice versa. After informal review by the editors, they may be published within a few months of the date of receipt. Style requirements are the same as for regular contributions (see inside back cover).

Large-Eddy Simulation of Rough-Wall Turbulent Boundary Layers

Changhoon Lee*
Yonsei University, Seoul 120-749, Republic of Korea

I. Introduction

THE rough-wall turbulent boundary layer has long been a research subject due to its consequences in real engineering practice and in its applications to the planetary boundary layer. Mainly experimental studies have been conducted to investigate the effect of roughness elements on turbulence structures in the outer layer, as well as on the mean flow.[1–4] In most experiments, suppression of a viscous sublayer and the downward shift of the log profile were commonly observed for a variety of roughnesses. Townsend's similarity hypothesis[5] (also see Ref. 2) states that the turbulent flow in the region outside the roughness sublayer is independent of the wall roughness and the viscosity, except for the role of the wall in setting the velocity scale u_τ at sufficiently high Reynolds numbers. A consequence is that, provided that the Reynolds number is sufficiently large, vertical profiles of turbulence intensities should collapse to common curves independent of wall roughness when normalized with u_τ and the boundary-layer thickness.[2] Previous measured data supported the similarity hypothesis.[6,7] In recent experimental studies,[3,4] however, it has been reported that the wall-normal component of turbulence intensity, when normalized by the wall-shear velocity, significantly increases, making the hypothesis questionable.

As a preliminary numerical investigation, a series of large-eddy simulations of rough-wall turbulent channel flows were carried out in this study. From the numerical point of view, simulation of rough-wall boundary-layer flow is a challenging problem because, despite recent advances in computer and numerical methods, an exact representation of a three-dimensional rough surface in numerical simulation is still almost impossible. To circumvent this problem, a roughness model was proposed, also known as the canopy model, in the simulation of the planetary boundary layer over a rough terrain, which distributes an arbitrary forcing opposite to local velocity in the near-wall region.[8,9] In the present numerical study, the so-called the virtual boundary method was adopted to represent a rough surface.[10,11] This method employs a feedback forcing to approximate the no-slip condition at the desired immersed surface present inside a flow domain without resorting to a complicated body-fitted coordinate transform. This method has been tested in a couple of turbulent flows, including turbulent channel flow over a riblet surface[12] or transitional flow around a sphere,[13] and, thus, the method was not fully validated in turbulent environments. However, when the performance of the method is considered in such cases, it is worthwhile to test the method in rough-wall turbulent flow simulations.

Received 25 March 2002; accepted for publication 9 June 2002.

*Associate Professor, School of Mechanical Engineering, 134 Shinchon-dong, Seodaemun-gu.

Furthermore, for the simulation of a rough-wall boundary layer in the fully rough regime, large-eddy simulation (LES) appears to be an only adequate method because direct numerical simulation (DNS) is restricted to low Reynolds numbers, whereas the Reynolds averaged Navier–Stokes model cannot provide detailed information of near-wall turbulence structures and cannot handle flow separation properly. Although modification of the subgrid-scale model near a rough surface in LES is not straightforward, a simple specification of the mixing length scale appears to be the first step toward a more accurate simulation.

II. Numerical Methods

A channel geometry with the size of $(4\pi, 2, \text{and } 4\pi/3)h$ in the streamwise, wall-normal, and spanwise directions, respectively, was selected, where h is the half gap of the channel. Periodicity in the streamwise and spanwise directions was assumed. A spectral method using Fourier expansions in the homogeneous directions and the Chebyshev expansion in the wall-normal direction was adopted. Three different resolutions, ($N_x = 32$, $N_y = 65$, and $N_z = 32$), ($N_x = 32$, $N_y = 97$, and $N_z = 32$), and ($N_x = 32$, $N_y = 97$, and $N_z = 64$), were used for $Re_\tau^{\text{base}} = 195$, 364, and 508, respectively. Here, x, y, and z denote the streamwise, wall-normal, and spanwise directions, respectively, and N_x, N_y, and N_z are the grid numbers in the respective directions. Re_τ^{base} is the Reynolds number based on the wall-shear velocity and h for the flow with a smooth wall, which is used as the base flow in rough-wall calculations. For the temporal integration of nonlinear terms, a third-order Runge–Kutta scheme was adopted, whereas linear terms were integrated using the Crank–Nicolson scheme.

For a subgrid-scale model, the Smagorinsky eddy viscosity model, $\nu_t = l^2 S$, was selected, where S is the representative rate of strain constructed from the fluctuation rate of strain, $S = \sqrt{(2S'_{ij}S'_{ij})}$, therefore allowing the eddy viscosity to approach zero for laminar flow. The length scale l was constructed by an arbitrary blending of two length scales:

$$1/l = 1/C_s\Delta + 1/\kappa y[1 - \exp(-y^+/A)] \tag{1}$$

where $\Delta \equiv (\Delta x\, \Delta y_{\max}\, \Delta z)^{1/3}$ and y is the distance from the wall. The optimum value of C_s was found to be 0.07 from the comparison with DNS data. The van Driest constant A is 26. This specification provided a good approximation of the length scale near a smooth wall, whereas for a rough wall simulation, the exponential correction was not made, permitting the length scale to behave linearly with the distance from the wall. Therefore, we did not intentionally incorporate the effect of roughness into the subgrid-scale model near the wall. This is based on the assumption that the effect of roughness can be mostly captured by the resolved-scale motion through an approximate representation of roughness geometry by the virtual boundary method.

For the satisfaction of the no-slip condition at the three-dimensional rough surface, the following virtual forcing is added to the right-hand side of the Navier–Stokes equations:

$$f_i = \alpha \int^t U_i(X_s, t')\, \mathrm{d}t' + \beta U_i(X_s, t) \tag{2}$$

where U_i is the fluid velocity at the immersed surface points X_s, which are distributed over the surface of roughness elements. The rough wall surface used in this study is illustrated in Fig. 1. Note that

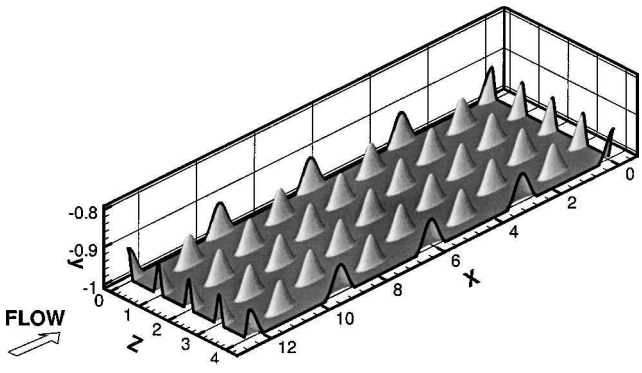

Fig. 1 Rough-wall surface used in LES.

the wall-normal scale is enlarged for a better view. The linear interpolation in three dimensions was used to obtain this velocity, and the computed force in the form of a delta function was spread back to the nearby mesh points using appropriate weights. Therefore, the uncertainty of the location of a roughness element associated with this approach is $(\Delta x, \Delta y, \Delta z)$ in each direction. Previous studies showed that the flow a few grids away from the virtual boundary points is not significantly influenced by this error.[11] Because α and β are negative real numbers of large magnitude, it is expected that the velocity at the surface of the roughness element will remain close to zero; $\alpha \Delta t_{\max}^2 = 50$ and $\beta \Delta t_{\max} = 5$ for all cases. The number of the immersed surface points distributed over the whole roughness elements ranges from 46,112 to 82,720.

Overall, the uncertainty in the predicted velocity occurs from two sources. One is from the incompleteness of the subgrid-scale model and the other is from the virtual boundary method in the representation of a rough surface. The uncertainty involved in the subgrid model in the roughness region is really difficult to quantify. To resolve this, a subgrid-model study accompanied by DNS would be necessary. However, the uncertainty occurring from the use of the virtual boundary method is due to the ambiguity of the location of roughness elements within one grid distance and the residual velocity at the virtual surface. A typical order of the residual velocity at the virtual surface is $0.01u_\tau$, which is relatively large considering that the no-slip condition is expected there. According to Saiki and Biringen,[11] the flow a few grids away from the virtual surface is not sensitively influenced by the location of, and the residual velocity at, the virtual surface in laminar environment. It is not clear that the same insensitivity holds for turbulence cases. Therefore, all of the turbulence data were extracted in the region two roughness heights away from the wall in our study.

III. Results and Discussion

Before implementing a rough surface, a smooth-wall turbulent channel flow was simulated using LES, and the results are compared with those obtained by the filtered DNS with enough resolution. Mean velocity and turbulence intensities are compared in Fig. 2. $Re_\tau = 200$, and the resolutions are $32 \times 65 \times 32$ and $128 \times 129 \times 128$ for the LES and DNS, respectively. A range of C_s was tested, and the choice of $C_s = 0.07$ produced the best result in terms of mean velocity. The general trend is that the higher value of C_s produces the smaller wall-shear stress, resulting in the greater elevation of the log profile. Agreement in the mean velocity is excellent. The streamwise intensity, however, is a little overpredicted, whereas the other components are underpredicted. Overall, agreement is relatively good considering that a simple subgrid model is adopted with one tuning parameter. When the total rates of strain were used in the evaluation of S instead of the disturbance rates of strain, the performance of LES was not good.

For all rough-wall calculations, the same rough-wall geometry as shown in Fig. 1 was used with a variety of roughness heights. All cases we tested are listed in Table 1. The height of a roughness element ranges from 0 to $0.14h$, and the corresponding value in wall units for each case, k^+, is also listed in Table 1. The range of k^+ covers the fully rough regime ($k^+ > 60$) for $Re_\tau^{\text{base}} = 364$ and 508,

Table 1 Computation cases

	$Re_\tau^{\text{base}} = 195$[a]			$Re_\tau^{\text{base}} = 364$[b]			$Re_\tau^{\text{base}} = 508$[c]		
k/h	k^+	Re_τ	ΔU^+	k^+	Re_τ	ΔU^+	k^+	Re_τ	ΔU^+
0.04	9	226	2.9	18	460	4.8	26	639	5.3
0.06	15	250	4.8	32	527	7.3	43	724	7.4
0.08	22	273	6.5	46	577	8.8	64	802	9.3
0.10	30	302	8.1	62	620	9.8	86	861	10.4
0.12	40	330	9.5	80	668	10.9	111	929	11.5
0.14	50	357	10.6	102	730	12.1	138	989	12.4

[a] $N_x = 32$, $N_y = 65$, and $N_z = 32$.
[b] $N_x = 32$, $N_y = 97$, and $N_z = 32$.
[c] $N_x = 32$, $N_y = 97$, and $N_z = 64$.

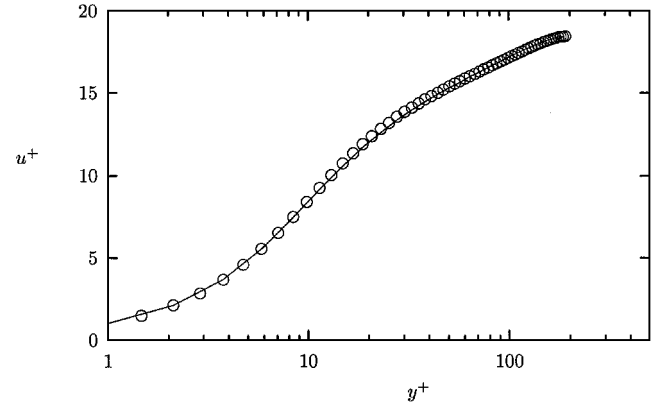

a)

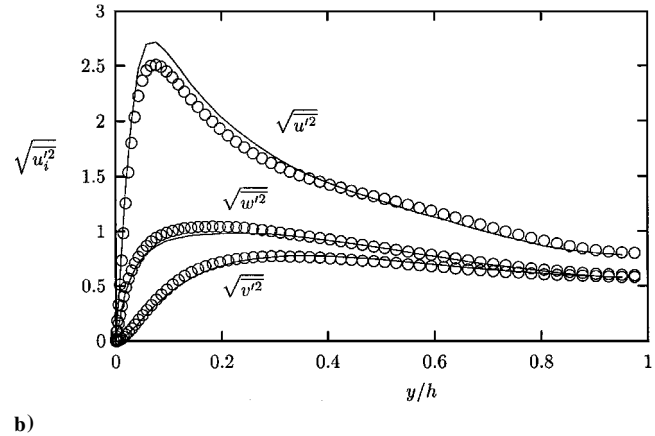

b)

Fig. 2 Smooth-wall case: ——, LES with a resolution of 32 × 65 × 32; ○, DNS with 128 × 129 × 128; and $Re_\tau = 200$ for a) mean velocity and b) rms velocities.

as well as the transitionally rough regime. Reynolds number Re_τ is based on the wall-shear velocity, which is obtained by integrating all of the surface force over the roughness elements, as well as the flat region between them. The other wall is maintained smooth to minimize the blockage effect or low Reynolds number effect.

Investigation of mean velocity distribution reveals that typical downward shifts of the log profile are observed for all cases, without the change in slope. The shift of the log profile known as the roughness function ΔU^+ for each case is listed in Table 1 and illustrated with known measured data for mesh screen or rod-type roughness in Fig. 3. The Prandtl–Schlichting scaling relation for sand-grain roughness (see Ref. 14), $1/\kappa \ell n k^+ - 3.0$, and an experimental fit for rod roughness,[4] $1/\kappa \ell n k^+ + 1.2$, are drawn together for comparison. Although most measured data reported were of a rough-wall turbulent boundary layer, which is different from channel flow, the range of ΔU^+ is quite comparable. The roughness geometry in our study is different from sand grain, mesh screen, or rod. The effect of roughness, however, appears to be rather similar to that of mesh screen or rod. In the fully rough regime ($k^+ > 60$), however, a constant slope of $1/\kappa$ is not observed in our simulation results. Furthermore,

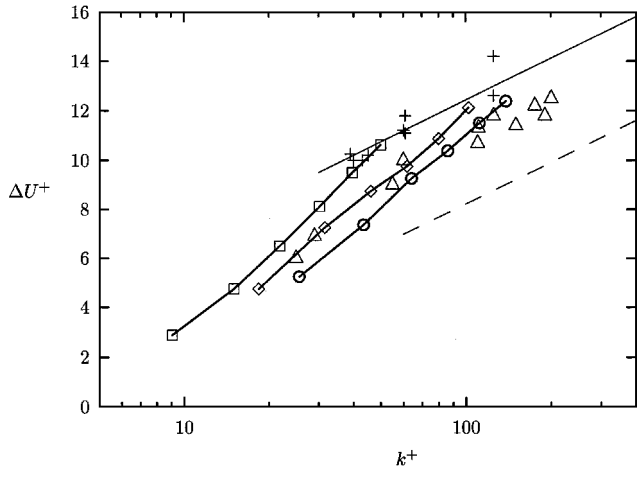

Fig. 3 Roughness function, ΔU^+: □, $Re_\tau^{\text{base}} = 195$ and $Re_\tau = 226 \sim 357$; ◇, $Re_\tau^{\text{base}} = 364$ and $Re_\tau = 460 \sim 730$; ○, $Re_\tau^{\text{base}} = 508$ and $Re_\tau = 639 \sim 989$; +, Krogstad and Antonia,[4] rods, $Re_\tau \geq 2000$; △, Krogstad et al.,[3] mesh screen $Re_\tau \geq 5200$; ——, $1/\kappa \ln k^+ + 1.2$ (Krogstad and Antonia,[4]); and – – –, $1/\kappa \ln k^+ - 3.0$ (Prandtl–Schlichting formula for sand-grain roughness; see Schlichting,[14]).

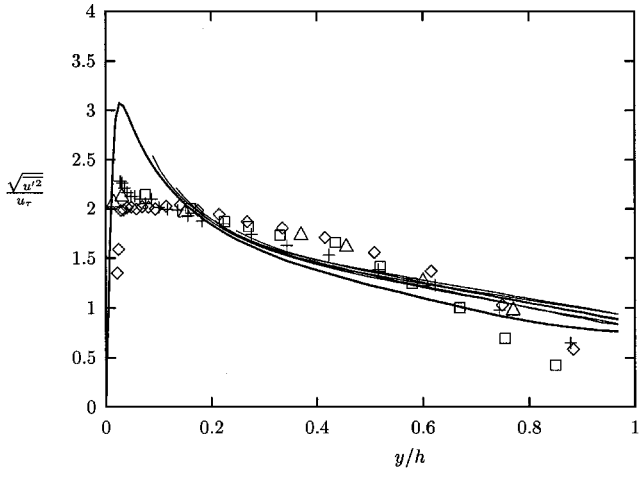

a)

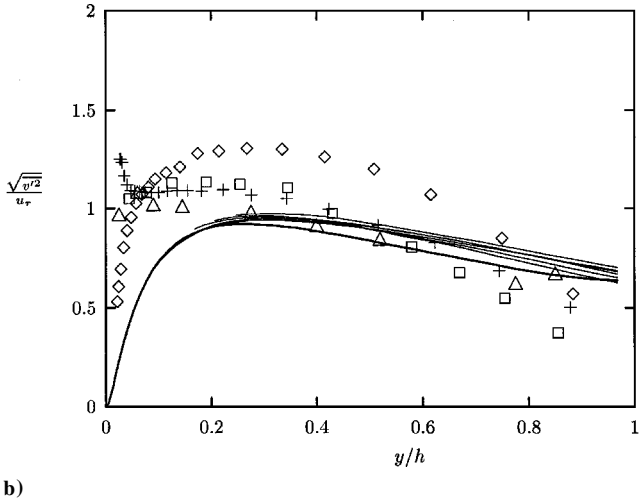

b)

Fig. 4 $Re_\tau^{\text{base}} = 508$: ——, smooth wall; ——, $k^+ = 26$, 43, 64, 86, 111, and 138; +, Krogstad and Antonia,[4] smooth wall; ◇, Krogstad and Antonia,[4] rods; □, Raupach,[6] vertical cylinders; and △, Andreopoulos and Bradshaw,[7] sand grain for a) $\sqrt{(u'^2)}/u_\tau$ and b) $\sqrt{(v'^2)}/u_\tau$.

the roughness functions for $Re_\tau^{\text{base}} = 195$, 364, and 508 do not collapse on one curve. However, as the Reynolds number increases, this roughness function seems to approach a fixed distribution. This inconsistency is most likely attributable to the blockage effect due to the presence of the other wall, which becomes dominant as the Reynolds number decreases or the roughness height increases. Unlike the boundary layer with the fixed freestream velocity, channel flow is subject to the constant-mass flux condition. This is believed to contribute to the increase of the wall-shear stress, thus causing the shift to be overpredicted.

The rms velocities normalized by the wall-shear velocity of the rough wall for various roughness heights at $Re_\tau^{\text{base}} = 508$ are shown in Fig. 4 with those for the smooth-wall case and known measured data for comparison. For the rough-wall cases, the rms distributions two roughness heights away from the wall are illustrated. It can be clearly seen that both the streamwise and wall-normal components in our simulation collapse on one curve in the region investigated regardless of roughness heights. In the outer region, the intensities for the rough-wall cases are slightly increased over the smooth-wall case. For the streamwise component, the measured data also exhibit universal behavior, independently of roughness type. Discrepancy between the measured data and our simulation is mainly due to different Reynolds numbers. (The range of Re_τ is $500 \sim 1000$ in our cases and $Re_\tau > 2000$ for the measured data.) However, the normal component shows a scatter. The measurements by Raupach[6] and Andreopoulos and Bradshaw[7] do not show much different distribution than the smooth-wall case, whereas Krogstad and Antonia's[4] data exhibit a substantial increase in the outer region. Although the rms quantities in LES are only for the resolved-scale motion, the contribution from the filtered scale is usually very small, especially at low Reynolds numbers. This collapse supports the similarity hypothesis. One may argue that the blockage effect possibly suppresses the normal component while redistributing energy to the streamwise and spanwise components. However, it turns out that this is not the case. If it were the case, then the normal component would be suppressed more for the lower-Reynolds-number case. Investigation of the results for $Re_\tau^{\text{base}} = 195$ reveals the opposite, that is, the normal component increases rather slightly with the roughness height. When viscosity and the wall-shear velocity are used to normalize intensities, no good collapse was observed. This suggests that the scaling parameters for rough-wall boundary-layer flow are the wall-shear velocity and the distance from the wall, thus excluding viscosity.

IV. Conclusions

Large-eddy simulations of rough-wall channel flow were carried out using the virtual boundary method to represent a rough surface. Typical downward shifts in mean velocity profile in the log region were observed with no variation of the slope. The amount of the shift for various roughness heights lies in the range of experimental scatter. Investigation of the rms velocities reveals that the wall-shear velocity scales the velocity well, thus supporting the similarity hypothesis. However, major drawbacks in our simulation are the uncertainty of the subgrid-scale model in the roughness region and a lack of validity of the virtual forcing method in turbulence simulation. Therefore, it is still not clear that the similarity hypothesis is invalid. Our study should be regarded as a first step toward more refined simulations of rough-wall turbulent flows. We are currently investigating the performance of the virtual boundary method in turbulence simulation.

Acknowledgments

This work has been supported by Yonsei University through Grant 2001-1-0118. We are grateful to an anonymous referee for fruitful comments and P.-Å. Krogstad for providing us with experimental data.

References

[1] Bandyopadhyay, P. R., and Watson, R. D., "Structure of Rough-Wall Turbulent Boundary Layers," *Physics of Fluids*, Vol. 31, No. 7, 1988, pp. 1877–1883.

[2] Raupach, M. R., Antonia, R. A., and Rajagopalan, S., "Rough-Wall Turbulent Boundary Layers," *Applied Mechanics Review*, Vol. 44, No. 1, 1991, pp. 1–26.

[3]Krogstad, P.-Å., Antonia, R. A., and Browne, L. W. B., "Comparison Between Rough- and Smooth-Wall Turbulent Boundary Layers," *Journal of Fluid Mechanics*, Vol. 245, 1992, pp. 599–617.

[4]Krogstad, P.-Å., and Antonia, R. A., "Surface Roughness Effects in Turbulent Boundary Layers," *Experiments in Fluids*, Vol. 27, No. 5, 1999, pp. 450–460.

[5]Townsend, A. A., *The Structure of Turbulent Shear Flow*, Cambridge Univ. Press, Cambridge, England, U.K., 1976, p. 139.

[6]Raupach, M. R., "Conditional Statistics of Reynolds Stress in Rough-Wall Turbulent Boundary Layers," *Journal of Fluid Mechanics*, Vol. 108, 1981, pp. 363–382.

[7]Andreopoulos, J., and Bradshaw, P., "Measurements of Turbulence Structure in the Boundary Layer on a Rough Surface," *Boundary-Layer Meteorology*, Vol. 20, No. 2, 1981, pp. 201–213.

[8]Miyake, Y., Tsujimoto, K., and Nakaji, M., "Direct Numerical Simulation of Rough-Wall Heat Transfer in a Turbulent Channel Flow," *International Journal of Heat and Fluid Flow*, Vol. 22, No. 3, 2001, pp. 237–244.

[9]Brown, A. R., Hobson, J. M., and Wood, N., "Large-Eddy Simulation of Neutral Turbulent Flow over Rough Sinusoidal Ridges," *Boundary-Layer Meteorology*, Vol. 98, No. 3, 2001, pp. 411–441.

[10]Goldstein, D., Handler, R., and Sirovich, L., "Modeling a No-Slip Flow Boundary with an External Force Field," *Journal of Computational Physics*, Vol. 105, No. 2, 1993, pp. 354–366.

[11]Saiki, E. M., and Biringen, S., "Numerical Simulation of a Cylinder in Uniform Flow: Application of a Virtual Boundary Method," *Journal of Computational Physics*, Vol. 123, No. 2, 1996, pp. 450–465.

[12]Goldstein, D. B., and Tuan, T.-C., "Secondary Flow Induced by Riblets," *Journal of Fluid Mechanics*, Vol. 363, 1998, pp. 115–151.

[13]Saiki, E. M., and Biringen, S., "Spatial Numerical Simulation of Boundary Layer Transition: Effects of a Spherical Particle," *Journal of Fluid Mechanics*, Vol. 345, 1997, pp. 133–164.

[14]Schlichting, H., *Boundary Layer Theory*, 7th ed., McGraw–Hill, New York, 1979, p. 616.

P. R. Bandyopadhyay
Associate Editor

Computational Simulation of the Air Wake over a Naval Transport Vessel

Martin J. Guillot*
University of New Orleans, New Orleans, Louisiana 70148

Introduction

NAVAL amphibious assault vessels transport personnel to and from operational areas. This is normally accomplished by operating some type of aircraft, for example, helicopters, from the deck of personnel transport ships. The ship topside structures produce an air wake over the deck in the operating region of the aircraft. The air wake is inherently unsteady due to vortex shedding from the topside structures. To understand the air wake and its possible effect on aircraft operations, it is necessary to quantify its main features. This Note presents time-averaged results of an unsteady computational simulation over a naval transport vessel. Experimental data are used to assess the accuracy of the computational results.

Previous researchers have computed the steady-state air wake over ships using various methods. For example, Tai and Carico[1] use a thin-layer Navier–Stokes method to compute the steady-state solution for the air wake over a landing helicopter deck (LHD) ship configuration. However, there is debate as to how to interpret results produced by a steady-state model when comparing to experimental data that was collected in a flowfield exhibiting global unsteadiness and then time averaged. Dolling[2] addresses this topic within the context of the supersonic compression ramp problem. Reynolds-averaged Navier–Stokes (RANS) computational fluid dynamics (CFD) models of supersonic compression ramps for large ramp angles where flow separation and reattachment occurs have historically shown poor agreement with experimental data for quantities such as mean surface pressure distribution and mean velocity profiles downstream of reattachment.[3–5] Dolling[2] asserts that the experimental flowfield exhibits global unsteadiness that is not captured by the steady-state solutions produced by RANS codes. He presents evidence indicating that better agreement with time-averaged experimental data might be obtained by a CFD computation that includes the global unsteadiness in the flowfield and then time averaged in the same manner as the experimental data.

In this effort, an unsteady computational simulation is performed on the topside airflow over a naval transport vessel. The results are time averaged, and the mean flow is compared to unsteady experimental data collected at the same frequency and time averaged in the same manner. Results are presented at selected points in the air wake over the aft deck of the vessel.

Experimental Study

In conjunction with the computational study, an experimental investigation into the air wake over a naval transport vessel was performed on a 1/94 subscale model in the 8 × 10 Foot Subsonic Wind Tunnel at the Naval Surface Warfare Center, Carderoc Division. The details of the experimental setup, procedures, data reduction, and results are reported by Guillot and Walker.[6] Data were collected at 500 Hz for 4.096 s.

The experimental accuracy is determined postexperiment by examining the mean square error in each probe's calibration curve, combined with an analysis of data taken at a freestream reference point during each run. The freestream reference point analysis is meant to account for individual probe response, which can change due to dirt accumulation on the sensor, plus any residual effects from ambient temperature variations. The expected confidence in the experimental data is ±5%.

Computational Simulatons

The ship geometry and coordinate system used in the computations are shown in Fig. 1. There are two helicopter landing pads on the aft deck, located at $x = 153.5$ and 188.0 m. The results presented here focus on the aft landing pad, $x = 188.0$ m and on the ship centerline.

The computational analysis was performed using FAST3D.[7] FAST3D, developed at the U.S. Naval Research Laboratory, is capable of solving the three-dimensional unsteady compressible Euler equations on parallel architectures using Cartesian meshes. It employs the flux-corrected transport method with virtual cell embedding to resolve internal boundaries in the flowfield.

Wind angles of 0 and 30 deg with respect to the ship centerline were studied with a nominal incoming velocity of 30 kn (15.34 m/s). To complete the description of the computational model, appropriate boundary conditions were prescribed. The locations of lateral boundaries were chosen to match the dimensions of the wind tunnel. The forward boundary was chosen to be one ship length ahead

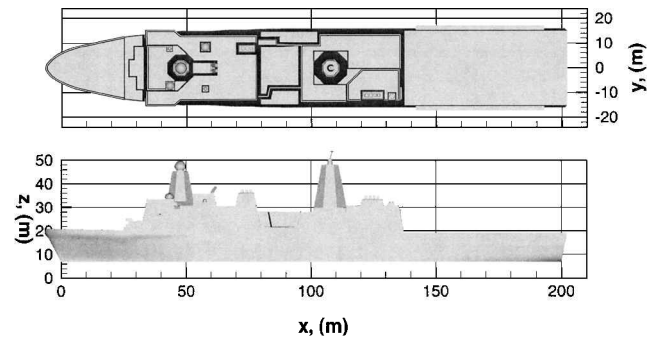

Fig. 1 Ship geometry and coordinate system.

Received 1 November 2001; revision received 15 December 2001; accepted for publication 9 June 2002.

*Assistant Professor, Department of Mechanical Engineering, 2000 Lakeshore Drive.